Journal of Power Sources 191 (2009) 465–472

Contents lists available at ScienceDirect

Journal of Power Sources

journal homepage: www.elsevier.com/locate/jpowsour

Silver–chromium oxide interactions in SOFC environments

Stephen W. Sofie[a,*], Paul Gannon[b], Vladimir Gorokhovsky[c]

[a] Mechanical and Industrial Engineering, Montana State University, 220 Roberts Hall, Box 173800, Bozeman, MT 59717, United States
[b] Chemical and Biological Engineering, Montana State University, Bozeman, MT, United States
[c] Arcomac Surface Engineering, LLC, Bozeman, MT, United States

ARTICLE INFO

Article history:
Received 3 January 2009
Received in revised form 13 February 2009
Accepted 13 February 2009
Available online 28 February 2009

Keywords:
SOFC
Silver
Silver chromite
Contact paste
Interconnect

ABSTRACT

Interactions between silver and chromium oxide were investigated during SOFC-relevant extended exposures pertaining to secondary phase formation and associated electrical contact degradation. In one case, Ag or Ag_2O and Cr_2O_3 powders were mixed, pressed into pellets and thermally treated in air at 700 °C, 800 °C and 900 °C for up to 1000 h. X-ray diffraction revealed $AgCrO_2$ and trace Cr_2O_3 in the specimens treated at 700 °C and 800 °C; however, Cr_2O_3, Ag and only trace amounts of $AgCrO_2$ were detected at 900 °C. In another case, silver contact paste was used in area specific resistance (ASR) measurements of ferritic stainless steel (FSS), with and without $(Co,Mn)_3O_4$ coatings, in 800 °C air for greater than 1500 h. A distinct reaction layer, having $AgCrO_2$ stoichiometry, was observed to form between the Cr-containing corrosion-products on the uncoated FSS and the silver contact paste yielding a 500% increase in ASR over 1500 h. No significant chemical interactions and ASR losses were observed with the $(Co,Mn)_3O_4$ coated FSS at this interface. Analyses and implications of the observed interactions of Cr_2O_3 and Ag within SOFC cathode environments are presented and discussed.

1. Introduction

Silver metal exhibits many physical and chemical properties that are driving the development of silver based SOFC applications such as sealing approaches, interconnect alloys, and composite cathodes [1–9]. These properties including: high electrical conductivity, hydrogen dissociation and oxidation catalysis, noble metal oxidation resistance/chemical stability, and relatively low cost are also advantageous in the form of contact pastes for fabrication and developmental testing of SOFC components [10,11]. A key downfall to the use of silver is the low melting point (~962 °C), which is exacerbated by its substantial volatility under SOFC operating temperatures (e.g., 650–850 °C) [6–9,12]. Silver metal loss for braze applications has been shown to reach 2×10^{-9} g cm^{-2} s at 850 °C [12]. Given the nature of silver metal at these elevated temperatures, the effectiveness of seals, contacts, and interfaces may be substantially deteriorated after only short exposures to SOFC operation at these temperatures, thus mitigating the potential benefits of developing SOFC systems based on silver for long duration operation. The implications of silver reactions and transport therefore have the potential to convolute the performance and degradation characteristics of SOFC testing at component, cell and stack level.

In addition to silver, ferritic stainless steels (FSSs) have seen heavy integration into SOFC designs by virtue of their compatible thermal expansion coefficient, ease in fabrication and low cost. Planar SOFC designs often utilize a FSS interconnect (IC), which separates fuel and oxidant gasses and connect individual cells into a stack. During operation, a Cr_2O_3-based thermally grown oxide (TGO) layer forms and grows predominantly on the FSS IC/cathode interface, which leads to increased ASR and eventuates in TGO layer spallation. In addition, Cr-transport (from TGO layers in either or both solid and gas phases) into cathodes and cathode/electrolyte interfaces has been established as a mechanism for substantial SOFC stack performance degradation [13–18]. A variety of protective coatings and deposition techniques have been investigated for the FSS SOFC(IC) application. More promising coating compositions include various doped lanthanum chromite and manganite perovskites, e.g., $La_{1-x}Ca_xCrO_3$ and $La_{1-x}Sr_xMnO_3$, and various Co, Fe, Ni, Cu and/or Mn-containing spinels, e.g., $(Co,Mn)_3O_4$ and $(Cu,Mn)_3O_4$ deposited by a range of solution and vapor-based approaches including thermal or plasma spray, slurry coating and physical or chemical vapor deposition [13,15,17,19].

Inexpensive silver leads and contact pastes, foils, and meshes are often used in SOFC materials development, e.g., ASR testing of FSS SOFC(ICs), which may influence chromium transport, TGO layer growth and ASR depending upon the extent of reaction between chromia and silver. The negative effects of silver may diminish its benefits due to interfacial degradation in virtually all aspects of SOFC application in temperature ranges supporting a prevalence of

* Corresponding author. Tel.: +1 406 994 6299; fax: +1 406 994 6292.
E-mail address: ssofie@me.montana.edu (S.W. Sofie).

0378-7753/$ – see front matter © 2009 Elsevier B.V. All rights reserved.
doi:10.1016/j.jpowsour.2009.02.036

SOFC development from 700 °C to 900 °C. Therefore, the objective of this study was to investigate the interaction of chromia-based TGO layers based upon degradation of current collection as opposed to cathode/electrolyte activity. Further, a common IC coating, $(Co,Mn)_3O_4$, was also evaluated with respect to conductivity degradation to evaluate potential impacts for the primary application of Ag-containing contact pastes and seals. The study was designed to not only evaluate the use of silver in moderate temperature ranges, but also to explore the upper temperature limits of silver containing contacts, where maximum stack performance may be required. The chemical stability was determined by X-ray diffraction analysis of silver/silver oxide and chromium oxide powders, in addition to thermodynamic equilibrium simulation while conductivity loss was determined by ASR measurement of FSS joined with silver.

2. Experimental procedure

2.1. Thermodynamic modeling

Thermodynamic equilibrium calculations of experimental systems were performed using the TERRA program with pressure, temperature and composition as key constraints [20]. Calculations were made using silver and chromium in moist air (400–1000 °C) to evaluate equilibrium solid, vapor and gas species within the TERRA database, which includes most of the refractory compounds properties within SGTE and JANAF-NIST databases. In addition, an ideal solid solution model was employed to approximate mixing among known compounds and assess the potential influence on phase transitions.

2.2. Chemical reactivity

Chemical interaction studies were performed with powder mixtures using silver metal (Ag), silver oxide (Ag_2O), and chromium oxide (Cr_2O_3) powders as received (Alfa Aesar). The powders were mechanically mixed in de-ionized water utilizing an ultrasonic horn with the addition of 1 wt% Darvan C-N (R.T. Vanderbilt) as a dispersant. The samples were mixed for 5 min at 100 W power level to achieve homogeneous mixtures. The mixtures were then dried in a gravity convection oven and pressed into 1 cm diameter × 0.3 cm thick pellets uni-axially at 200 MPa for 1 min. Powder mixtures of Ag_2O/Cr_2O_3 and Ag/Cr_2O_3 were mixed at a 50/50 weight percent ratio and individual pellets from the same batch were heat treated under ambient air conditions (approximately 55% relative humidity) at 700 °C, 800 °C, and 900 °C on a high purity aluminum oxide substrate. Utilizing a heating rate of 5 °C min^{-1} the Ag_2O/Cr_2O_3 pellets were heat treated for 1000 h and the Ag/Cr_2O_3 pellets were treated for 500 h. Following thermal treatment, the pellets were ground in an aluminum oxide mortar and pestle and analyzed by powder X-ray diffraction (Scintag X1) for phase determination.

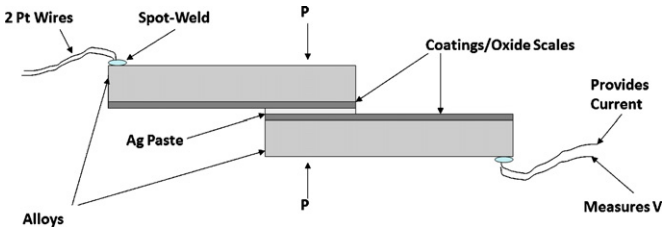

Fig. 1. Schematic representation of the 4-probe ASR measurement apparatus.

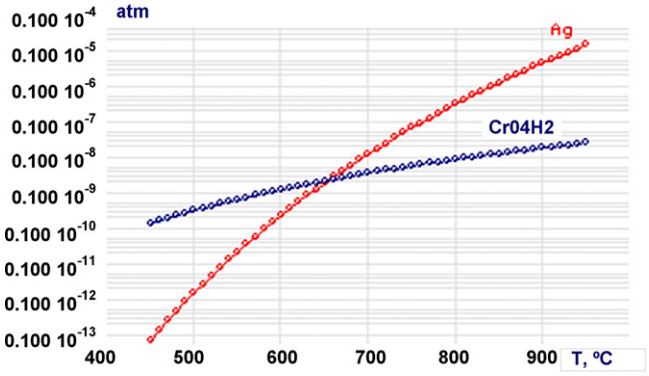

Fig. 2. Equilibrium vapor pressures of dominant Ag and Cr-containing vapor species in moist air (3 vol% H_2O) as a function of temperature.

ASR measurements were performed on coated and uncoated FSS (Crofer 22 APU) utilizing silver as a contact paste (Silver Conductive Ink, Alfa Aesar) in a standard four-point probe configuration shown in Fig. 1. A ~3 μm $(Co,Mn)_3O_4$–(Co:Mn = 1:1) protective spinel coating was applied to the FSS surface using a filtered arc-assisted electron beam physical vapor deposition process, a process described elsewhere [19]. Both coated and uncoated FSS test specimens were pre-oxidized in 800 °C air for 100 h prior to the ASR measurement. The measurements were performed at 800 °C under ambient conditions for up to 2000 h to evaluate the long term ASR behavior of coated and uncoated FSS in contact with silver. Following the measurements, ASR test specimens were cross-sectioned and polished for SEM/EDS analysis (Jeol 800).

3. Results

Thermodynamic equilibrium calculations considering an initial 1:1 mass ratio of Ag:Cr in air (3 vol% H_2O) were plotted in the temperature range from 400 °C to 1000 °C to cover the complete useful range of SOFC operation. Fig. 2 shows the volatilization behavior of Ag and Cr-containing species, which indicate substantial vapor pressures of $CrO_2(OH)_2$ and Ag at elevated temperatures [21]. Ther-

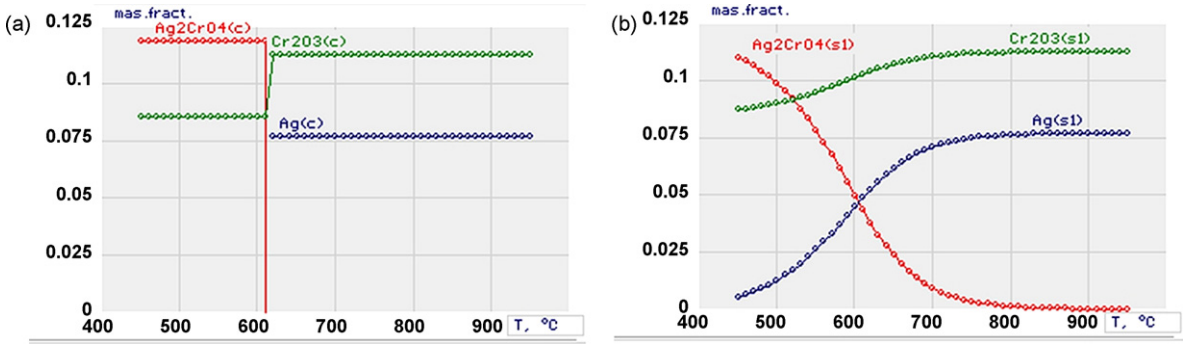

Fig. 3. Thermodynamic equilibrium mass fractions of Ag–Cr oxides in air as a function of temperature: (A) assuming immiscible solid compounds; (B) assuming ideal solid solution among Ag_2CrO_4, Ag and Cr_2O_3.

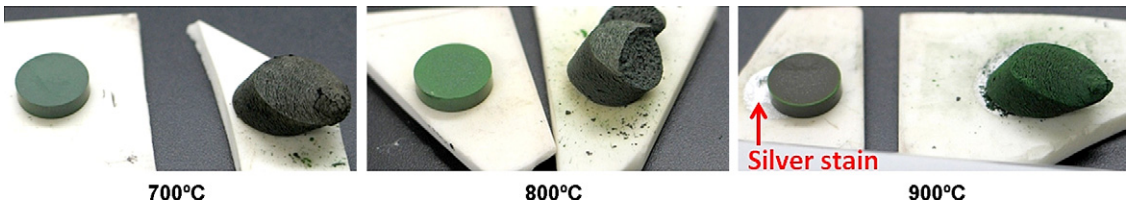

Fig. 4. Optical images of silver–chromia pellets after heat treatment (Ag/Cr_2O_3 left pellets, Ag_2O/Cr_2O_3 right pellets).

modynamic equilibrium mass fractions of condensed phase species vs. temperature are presented in Fig. 3. Fig. 3A assumes immiscibility among condensed phases and shows an abrupt decomposition of Ag_2CrO_4 into Ag and Cr_2O_3 at ~610 °C. Fig. 3B assumes an ideal solid solution among condensed phases and shows a gradual decomposition of Ag_2CrO_4 into Ag and Cr_2O_3, from ~500 °C to 700 °C. Both these simulations are consistent with experimental observations, including a measured melting temperature of Ag_2CrO_4 at ~665 °C [22–25]. Although no thermochemical data was available for $AgCrO_2$, this compound was observed experimentally, and therefore the ideal solid solution of Ag and Cr_2O_3 may account for its presence on a first-approximation for comparison to empirical data.

Fig. 4 shows optical images of silver/chromia and silver oxide/chromia pellets at respective temperatures, illustrating the dimensional change of the silver oxide based pellets, given the identical initial size of silver and silver oxide pellets. Further, silver staining of the aluminum oxide substrates is observed only for the pellets annealed in 900 °C air. The XRD patterns of the ground mixtures of Ag/Cr_2O_3 are shown in Fig. 5 and illustrate substantial secondary phase formation of $AgCrO_2$ in the 700 °C and 800 °C pellets as well as minimal retained secondary phase in the 900 °C specimens. Fig. 5 also indicates substantial silver content in the ground pellet after 900 °C thermal treatment. The XRD patterns of the ground mixtures of Ag_2O/Cr_2O_3 are also shown in Fig. 6 and illustrate substantial secondary phase formation of $AgCrO_2$ in the 700 °C and 800 °C pellets however in contrast to Fig. 5 only Cr_2O_3 is retained after 900 °C thermal treatment.

3.1. ASR testing

Cross-sections of silver joined resistivity couples (using Ag based contact paste) fabricated with and without the Mn–Co spinel thin film coating are shown in Fig. 7. The formation of manganese–chromium and silver–chromium secondary phases (evidenced by EDS analysis) is clearly evident yielding electronic conduction across the contact that is substantially reduced from the electrical conduction of pure silver. In addition, ASR vs. time

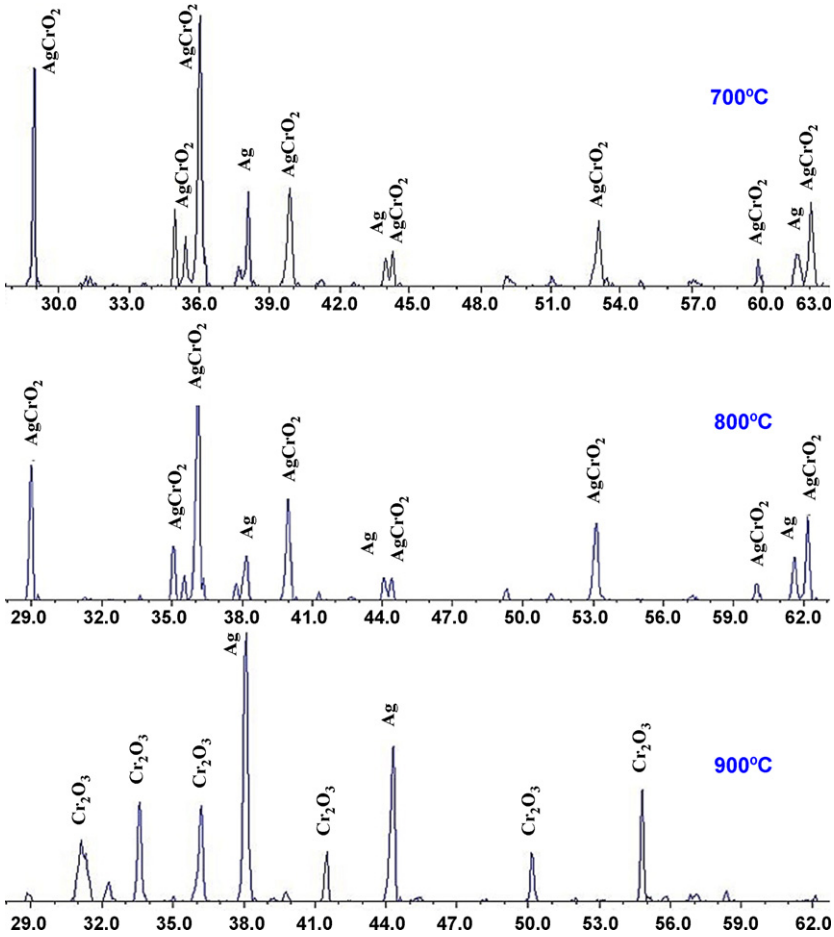

Fig. 5. XRD analysis of metallic Ag pressed pellets showing substantial formation of $AgCrO_2$ at 700 °C and 800 °C as well as minimal evidence of retained $AgCrO_2$ and increased retention of Ag at 900 °C.

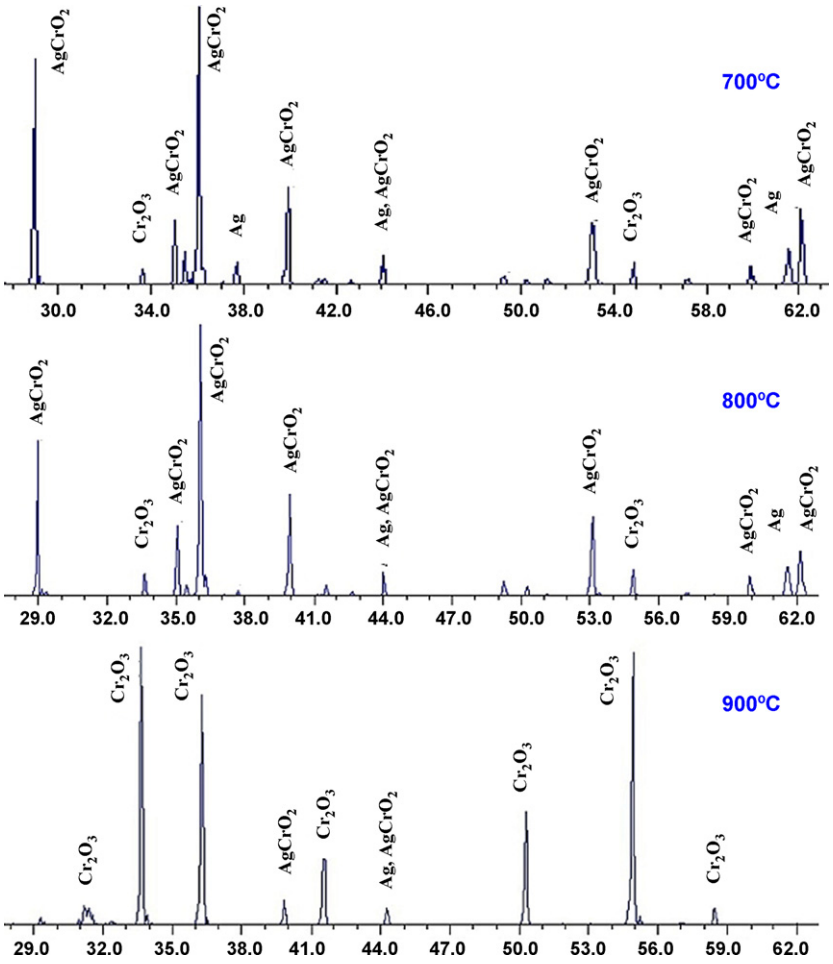

Fig. 6. XRD analysis of Ag_2O pressed pellets showing substantial formation of $AgCrO_2$ at 700 °C and 800 °C as well as minimal evidence of retained $AgCrO_2$ at 900 °C.

of coated and uncoated FSS at 800 °C is shown in Fig. 8 with SEM images and EDS line scans of test specimen polished cross-sections. The uncoated FSS grew a relatively thick (10–20 μm) Cr_2O_3-based TGO layer, which reacted with the Ag contact paste to form a distinct Ag–Cr oxide interfacial layer. In contrast, the ~3 μm FA-EBPVD $(Co,Mn)_3O_4$ coating did not react significantly with Ag contact paste, but formed a ~1–2 μm TGO layer at the coating/FSS interface during the 2000 h ASR test yielding a final coating/TGO layer thickness of ~4–5 μm.

4. Discussion

4.1. Thermodynamic modeling

The potential for Ag and Cr volatility under SOFC operating temperature is illustrated in Fig. 2, which shows appreciable and increasing equilibrium vapor pressure of $CrO_2(OH)_2$ and Ag in air at elevated temperatures. Compared with this simulation, Cr and Ag activities may effectively decrease in SOFC application when compounded with other metals and/or oxides. Regardless, the availability of silver and/or Cr-containing vapor may drive reactions with other components and create deleterious secondary phases. Further, the extent of volatilization and re-deposition has the potential to mask the degradation behavior of an electrode by deposition of fine silver electro-catalyst particulate within the electrochemically active regions of the cell.

The calculated equilibrium mass fractions of known Cr and Ag-containing species in moist air are presented in Fig. 3. Lower-temperature stable phases are Cr_2O_3 and Ag_2CrO_4, which form from the oxidation of chromium to form chromia, and the reaction of chromia with Ag and oxygen to form silver chromate, as shown in Eq. (1). This interaction behavior has also been observed in the literature [22–26].

$$8Ag + 2Cr_2O_3 + 5O_2 = 4Ag_2CrO_4 \quad (1)$$

Fig. 3 indicates that chromia and silver chromate coexist until ~600 °C. With increasing temperature, silver chromate further interacts with chromia in the formation of a new phase, silver chromite ($AgCrO_2$). The proposed reaction is shown in Eq. (2) and is based on subsequent chemical analysis by XRD (Fig. 5).

$$Ag_2CrO_4 + (1/2)Cr_2O_3 = 2AgCrO_2 + (3/4)O_2 \quad (2)$$

Because TERRA lacks thermodynamic data for $AgCrO_2$, an ideal solid solution among Ag_2CrO_4, Cr_2O_3 and Ag is used for estimation, which predicts the established reaction of silver chromate with chromia [22,25,26]. This provides an important basis for comparison and validation with empirical testing at discrete temperature steps by XRD. The silver chromite phase is found to be stable past 700 °C up to ≥800 °C (Fig. 6) at which point the chromite undergoes a decomposition reaction to form chromium oxide and silver, as shown in Eq. (3).

$$2AgCrO_2 = Cr_2O_3 + 2Ag + (1/2)O_2 \quad (3)$$

It appears that silver chromate is a stable secondary phase below ~650 °C when it begins to react with chromia (via Eq. (2)) to form silver chromite, which indicates hexavalent chromium (Cr^{6+}). This

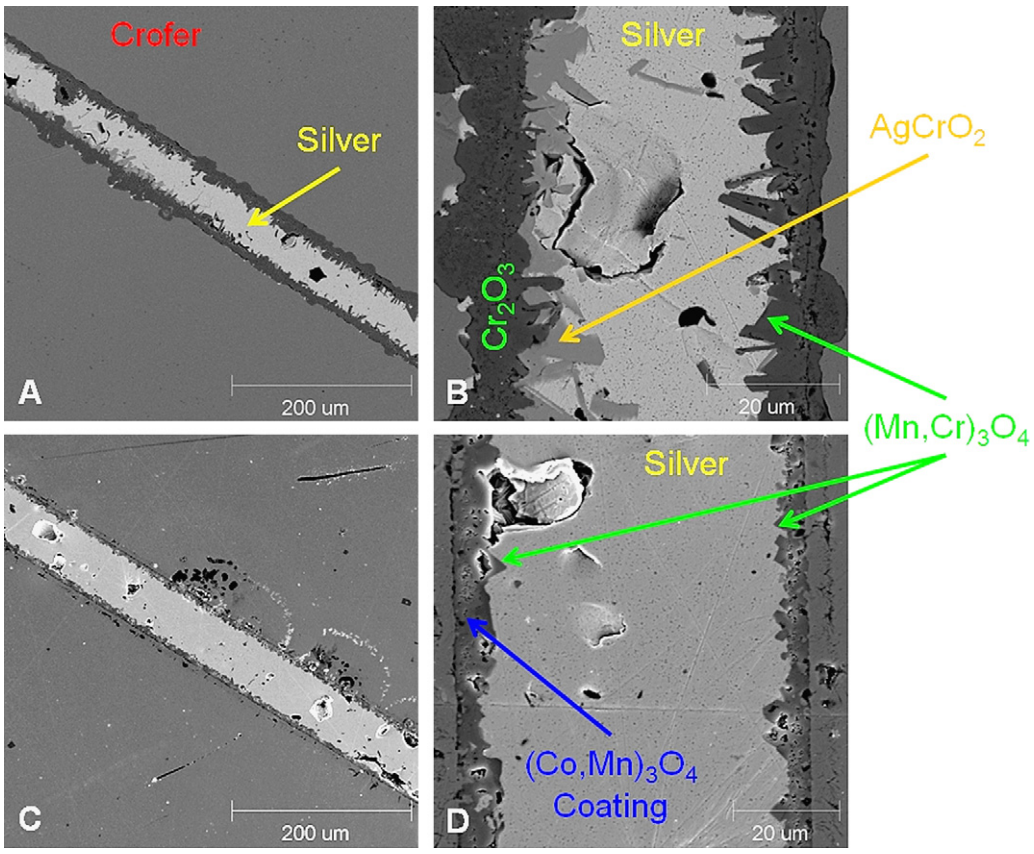

Fig. 7. Silver contacted ASR couples without $(Co,Mn)_3O_4$ barrier (A and B) and with $(Co,Mn)_3O_4$ barrier (C and D).

reaction appears complete by ~800 °C, above which leads to Ag and Cr_2O_3 by decomposition and that may volatilize and/or further react with other SOFC components forming additional secondary phases apart from the contact layer region. In this manner silver chromium oxides do not appear to effectively "lock up" the chromium over a broad temperature range as do the more stable manganese chromates and lanthanum chromites.

4.2. Chemical reactivity

Silver oxide was utilized to induce additional porosity in the pressed pellet to more closely resemble that which can be present in fuel cell contact paste/cathode applications requiring gas transport characteristics, whereas, higher density silver/chromia mixtures were utilized to reduce overall porosity of the pressed pellets. Silver oxide loses it affinity for oxygen at ~220 °C under ambient conditions in which the free energy of formation for silver oxide shifts to positive, thus resulting in the Ag_2O becoming thermodynamically unstable. The silver releases oxygen at this point, which results in the formation of the foam-like appearance of the silver oxide/chromia pellets as opposed to the dense silver/chromia pellets after thermal treatment. This behavior is shown in Fig. 4 as a growth and distortion of the original pellet dimensions due to oxygen degassing. Given the relatively fast heating rate and high density of the green pellet, the oxygen degassing process occurred in a manner such that the gas was not allowed sufficient time for release, thereby distorting the shape of the pellet. The use of silver oxide in lower density and reduced thickness contact pastes may not yield the extent of expansion seen in Fig. 4, but may serve as a mechanism to improve contact from this in situ expansion mechanism in between cell/interconnect components. However, whether starting with silver or silver oxide, the end result is a mixture of silver/chromia prior to chemical reaction with the key difference being the level of porosity, homogeneity of components, and exposed surface area. Observational examination of pellets in Fig. 4 does indicate some variation due to porosity, particularly at 900 °C, which suggests less retention of Ag metal in the silver oxide pressed pellets and hence more heavily retained Ag metal in the metallic silver pressed pellets.

Given the stoichiometric variation in reactants and retained primary phases, the XRD patterns of the 700 °C, 800 °C, and 900 °C tests for both the silver and silver oxide based pellets are shown in Figs. 5 and 6 to establish the secondary phase formation and decomposition characteristics of the powder mixtures. The XRD results in Figs. 5 and 6 indicate that for the 700 °C and 800 °C treated pellets the silver and chromia reacted to form the secondary phase of silver chromite, $AgCrO_2$. The chemical analysis indicates a silver chromite phase different from that of thermodynamic calculation (silver chromate in Fig. 3B) in which the balanced chemical reaction is shown in Eq. (2). Silver chromate was not detected by XRD scans, however, the 2–4% detection limit of XRD does suppress the means to accurately detect minor chromate phase. Further, in contrast to Eqs. (1) and (2), it is evidenced from the retained minor phases in Figs. 5 and 6 that substantially less oxygen pick-up, required to form the chromate phase, is evidenced from the experiments carried out in ambient atmospheric conditions. This phenomenon is attributed to limitations associated with atom transport as well as molar ratio variations in the reactant mixtures.

The retained minor phases, however, indicated some variation that appears to be driven by microstructural porosity difference of the thermally treated pellets. The dominant secondary $AgCrO_2$ dictates that a 1Ag:1Cr molar ratio of reactants, is required for complete chemical formation of $AgCrO_2$. The molar ratios of the 50–50 wt% reactant mixtures yielded a 0.65Ag:1Cr molar ratio for

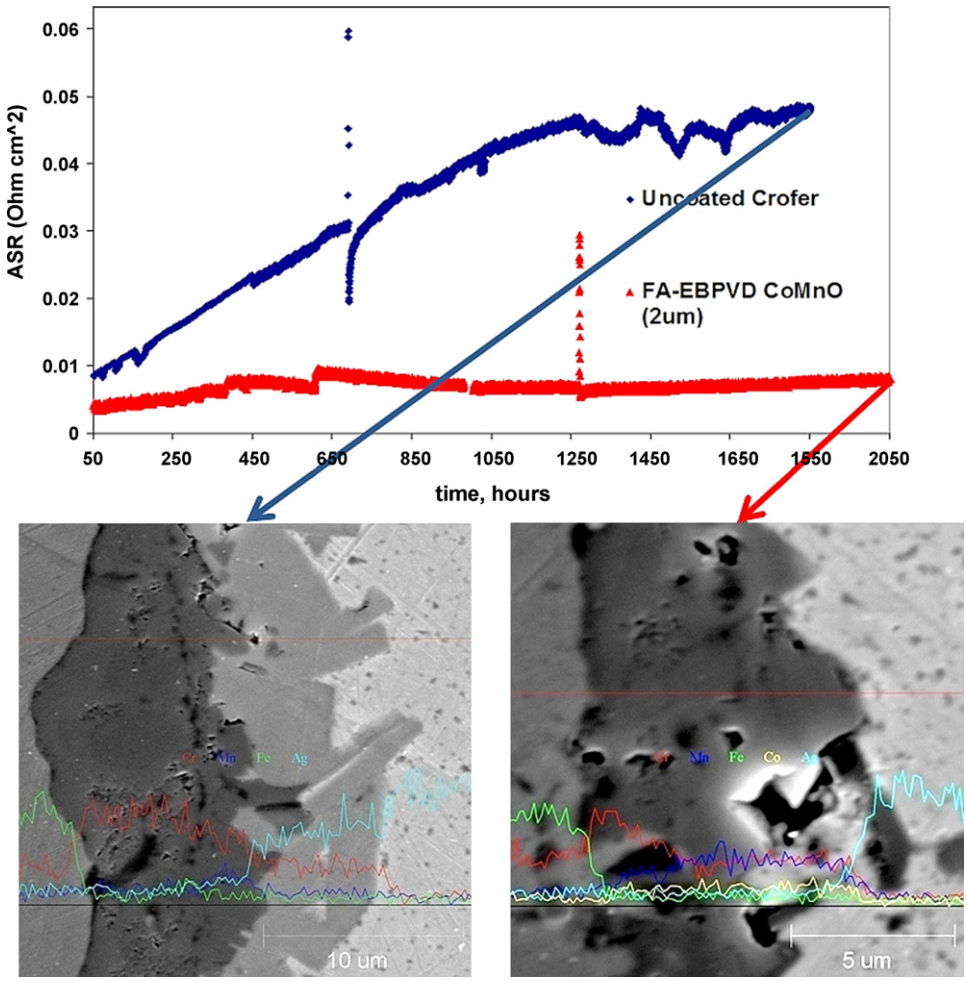

Fig. 8. ASR results of FSS/Ag sandwiches tested at 800 °C with post-testing SEM/EDS cross-section analysis.

the metallic silver pellets and a 0.70Ag:1Cr molar ratio for silver oxide pellets. The molar ratios used in both test batches indicates a deficiency of Ag which ideally should yield excess Cr_2O_3 and negligible retained silver, assuming the long durations were sufficient for long range atom transport. Examination of XRD patterns for temperatures below the decomposition regime for $AgCrO_2$ from 700 °C to 800 °C show that the metallic silver pellets have a substantial Ag minor phase (Fig. 5) while the silver oxide pellets indicate both Cr_2O_3 and Ag minor phase (Fig. 6). This suggests that short duration ultrasonic mixing may not yield complete homogenization of the mixtures, resulting in discrete regions of Cr_2O_3 and Ag separated by secondary chromite phase, thus providing a diffusion barrier. The temperature increase from 700 °C to 800 °C indicated a minimal change in the retention of minor phase(s) which further supports the formation of an effective diffusion barrier. The high vapor pressures of chromium oxy hydroxide and silver, Fig. 2, were not sufficient to provide chemical homogeneity over 1000 h of testing for which the relative porosity of the powder compact was intended to provide a closer link to the equilibrium simulation by providing vapor diffusion paths for more complete reaction. Empirically, these results indicate limited chemical interaction by vapor transport (evaporation/condensation), which is strongly temperature dependent based on the thermal stability of $AgCrO_2$ indicated previously by the thermodynamic simulation in Fig. 3B, further establishing the relevance of the ideal solid solution. Evidence of retained Ag in the metallic silver pellets may be attributed to the use of high density metallic silver particles that are prone to settling and decreased homogeneity in contrast to silver and chromium oxides, where $\rho_{Cr_2O_3} = 5.2\ g\ cm^{-3}$, $\rho_{Ag_2O} = 7.2\ g\ cm^{-3}$, and $\rho_{Ag} = 10.5\ g\ cm^{-3}$. Furthermore, the ammonium polymethacrylate dispersant, designed to disperse oxide powders, may not yield the most effective dispersion for metallic particles. In this manner large clusters of metallic silver may yield relatively small surface area for chemical reactivity and volatility.

As the temperature extends beyond 800 °C the instability and hence decomposition of $AgCrO_2$ results in Ag and Cr_2O_3 for which the elevated temperature promotes considerable chromium and silver volatility. This also supports the ideal solid solution treatment for Fig. 3B which predicts this behavior well. Therefore, ~800 °C marks an apparent transition for the long term stability of silver contacts which is evidenced by the XRD data in Fig. 6 for the 900 °C pellet, in which minimal $AgCrO_2$ phase is present with no evidence of retained silver metal. Upon decomposition of $AgCrO_2$, the silver metal is rapidly volatilized yielding phase pure Cr_2O_3. This contributes to the green, Cr_2O_3, color of the 900 °C silver oxide based pellet in Fig. 4. At lower temperatures between 700 °C and 800 °C, the secondary phase formation is the dominant process in which silver and chromia will readily react to form $AgCrO_2$. Based on the XRD and thermodynamic results, at temperatures below 800 °C, the $AgCrO_2$ phase appears to limit mass transfer by forming a continuous phase around residual Ag and Cr_2O_3, however, as the phase becomes unstable above 800 °C, the $AgCrO_2$ phase no longer acts as an effective vapor diffusion barrier. The 900 °C XRD pattern in Fig. 6 shows fewer trace compound peaks substantiating

this behavior. In contrast, Fig. 5 while also indicating trace $AgCrO_2$ phase at 900 °C, shows substantial retention of Ag metal. Given the vapor pressure of Ag at 900 °C, this retention is explained by the higher density of metallic silver based pellet in which vapor diffusion paths are limited compared to the highly porous silver oxide pellets.

While the near complete decomposition of the $AgCrO_2$ at 900 °C may indicate a region of chemical stability between Ag and Cr_2O_3, the volatilization rate and hence thermal stability of silver becomes unsuitable for long term operation. The silver staining of the alumina substrate during 900 °C thermal treatments further indicates the excessive volatilization of the silver seen in Fig. 4. Limiting and/or engineering porosity in silver based contacts may, however, provide a micro-structural means to facilitate thermochemical stability by limiting silver vapor transport (Fig. 5, 900 °C), which will be dependent upon the particle size/distribution, temperature, and duration of the thermal treatment.

4.3. ASR testing

The manganese, which intentionally alloyed with the FSS, is designed to form $(Mn,Cr)_3O_4$ spinel phase, to inhibit excessive chromia scale growth and spallation. Fig. 7 indicates exaggerated growth of the $(Mn,Cr)_3O_4$, evidenced in ASR samples post-testing, for which it is postulated that enhanced chromium transport through the silver accelerates the growth. SEM images in Fig. 7 are labeled with compositions that are assumed from XRD analysis, given that EDS only represents elemental concentration. The preferential growth, indicated by the acicular/dentritic formation of secondary phases, for both Ag and Mn chromium oxides indicate that specific crystallographic orientations are more favorable to chemical interaction. This anisotropy may be particularly attractive with the $(Mn,Cr)_3O_4$ system in which oriented coatings may be more effective growth barriers. The segregation of silver and manganese chromium oxides to opposite sides of the uncoated specimen in Fig. 7B is not understood, however, this may be attributed to preferential ion migration under a DC current. The polarity of the samples, however, was not preserved during the metallographic preparation. The extent of secondary phase growth in Fig. 7A and B, regardless of the deleterious effect on electronic conduction, presents a substantial concern for interface failure which is driven by differential thermal expansion and increasing interface stress as the oxides grow. While the silver chromite appears to inhibit vapor diffusion based on the previous discussion of XRD, migration of chromium into the contact by solid state diffusion yields an unfavorable growth of deleterious phases. The coated specimen in Fig. 7C and D, however, indicates negligible $AgCrO_2$ phase, yielding a predominantly phase pure silver contact. The formation of $(Mn,Cr)_3O_4$ clusters beyond the coating interface and growing into the silver contact in Fig. 7D further indicate that even high quality vapor deposited Mn–Co spinels are not 100% effective from inhibiting mass transfer of chromium from the underlying substrate.

The ASR results presented in Fig. 8 show a predictable rise in ASR vs. time for the uncoated FSS specimen resulting from the increasing chromia-based TGO layer thickness. ASR values fluctuate significantly after ~1250 h, which may be due to the formation of the observed Ag–Cr oxide layer at the interface of the chromia-based TGO layer and silver contact paste. The decreasing slope of the ASR curve suggests that the $AgCrO_2$ coating ultimately limits silver transport to the chromia scale interface; however, at this point the scale thickness is approaching 10 μm in some regions of the joint, which presents a substantial concern for spalling. Localized spalling and interface failure is indicative of the erratic ASR behavior past 1250 h testing for the uncoated specimen. On the other hand, the ~3 μm FA-EBPVD $(Co,Mn)_3O_4$ spinel coating is not only effective at minimizing chromia scale growth, the coating also negates chemical reactivity with the silver metal. This is supported by the abrupt silver concentration change in the EDS line scans in Fig. 8 indicated by the blue trace. While volatilization still presents a problem above 800 °C, the use of spinel coatings and the relative stability of $AgCrO_2$ may allow the use of silver based contact pastes and seals in the lower temperature regimes up to 800 °C.

5. Conclusions

The formation of silver chromite ($AgCrO_2$) is shown to be thermodynamically stable over the 700–800 °C temperature range, while the $AgCrO_2$ decomposes to Ag and Cr_2O_3 at temperatures above 800 °C, suggesting a temperature limit for SOFC operation using silver contacts/seals/leads with FSS interconnects. Temperatures above 800 °C indicate substantial metallic silver volatilization as observed by condensation on adjoining support substrates. Long duration testing, 500–1500 h, indicates a strong correlation between thermodynamic simulation and experimental testing of silver interaction with chromia. The formation of non-uniformly shaped secondary phases appears to be promoted by enhanced chromium migration with silver contacted FSS sandwiches, yielding accelerated oxide scale growth and increased ASR. While silver metal is shown to react extensively with chromia, the application of a FA-EBPVD $(Co,Mn)_3O_4$ spinel coating is shown to mitigate the formation of unstable and deleterious silver chromium oxide phases. The use of silver materials in the air side, particularly in the $AgCrO_2$ decomposition temperature regime, is shown to provide an additional mechanism of solid oxide fuel cell degradation, and may not be suitable for use in fundamental degradation studies or long term performance applications at both the cell and stack level.

Acknowledgements

This work was supported by the MSU-HiTEC program and is funded by the United States Department of Energy under Award No. DE-AC06-76RL01830. Any opinions, findings, conclusions, or recommendations expressed herein are those of the author(s) and do not necessarily reflect the views of the DOE.

References

[1] S.P. Simner, M.D. Anderson, J.E. Coleman, J.W. Stevenson, J. Power Sources 161 (1) (2006) 115–122.
[2] K.S. Weil, J.Y. Kim, J.S. Hardy, Electrochem. Solid-State Lett. 8 (2) (2005) A133–A136.
[3] C.C. Beatty, Proceedings-Electrochemical Society, v PV 2005-07, Solid Oxide Fuel Cells IX, SOFC IX: Materials-Proceedings of the International Symposium, 2005, pp. 1949–1956.
[4] M.C. Tucker, C.P. Jacobson, L.C. De Jonghe, S.J. Visco, J. Power Sources 160 (2) (2006) 1049–1057.
[5] S. Huang, Z. Zong, C. Peng, J. Power Sources 173 (1) (2007) 415–419.
[6] J. Duquette, A. Petric, J. Power Sources 137 (1) (2004) 71–75.
[7] M. Camaratta, E. Wachsman, Solid State Ionics 178 (19–20) (2007) 1242–1247.
[8] M. Camaratta, E. Wachsman, Solid State Ionics 178 (23–24) (2007) 1411–1418.
[9] J.Y. Kim, J. Hardy, K.S. Weil, Int. J. Hydrogen Energy 32 (16) (2007) 3655–3663.
[10] W.A. Meulenberg, O. Teller, U. Flesch, H.P. Buchkremer, D. Stover, J. Mater. Sci. 36 (13) (2001) 3189–3195.
[11] J. Liu, Y. Lu, S.A. Barnett, A. Ji, W. Su, Proceedings-Electrochemical Society, v PV2005-07, Solid Oxide Fuel Cells IX, SOFC IX, 2005, pp. 1976–1980.
[12] Z.G. Lu, J.H. Zhu, Electrochem. Solid-State Lett. 10 (10) (2007) B179–B182.
[13] J.W. Fergus, J. Hydrogen Energy 32 (16) (2007) 3664–3671.
[14] K. Ogasawara, et al., J. Electrochem. Soc. 154 (7) (2007) 657–663.
[15] M.C. Tucker, H. Kurokawa, C.P. Jacobsen, L. De Jonghe, S.J. Visco, J. Power Sources 160 (1) (2006) 130–138.
[16] S.P. Jiang, S. Zhang, Y.D. Zhen, J. Mater. Res. 20 (3) (2005) 747–758.
[17] M. Krumpelt, T.A. Cruse, M.C. Hash, Proceedings-Electrochemical Society, v PV 2005-07, Solid Oxide Fuel Cells IX, SOFC IX, 2005, pp. 1578–1583.
[18] C. Gindorf, L. Singheiser, K. Hilpert, Steel Res. 72 (11–12) (2001) 528–533.
[19] V.I. Gorokhovsky, P.E. Gannon, M.C. Deibert, R.J. Smith, A. Kayani, M. Kopczyk, D. Vanvorous, Z. Yang, J.W. Stevenson, S.J. Visco, C.P. Jacobson, H. Kurokawa, S.W. Sofie, J. Electrochem. Soc. 153 (10) (2006) A1886–A1893.

[20] N.A. Vatolin, G.K. Moiseev, B.G. Trusov, Metallurgy (1994).
[21] E.J. Opila, D.L. Myers, N.S. Jacobson, I.M.B. Nielsen, D.F. Johnson, J.K. Olminsky, M.D. Allendorf, J. Phys. Chem. A 111 (10) (2007) 1971–1980.
[22] B. Abu-Zied, Appl. Catal. A: Gen. 198 (1) (2000) P139–P153.
[23] Y. Niu, J.X. Song, F. Gesmundo, G. Farne, Oxid. Met. 55 (3–4) (2001) 291–305.
[24] H.W. Abernathy, E. Koep, C. Compson, Z. Cheng, M. Liu, J. Phys. Chem. C 112 (34) (2008) 13299–13303.
[25] C.W.F.T. Pistorius, J. Chem. Phys. 46 (1967) 2167–2171.
[26] M. Cieslak-Golonka, J. Wieckowska, B. Kacma, J. Therm. Anal. 36 (1990) 2217–2221.